

# Chapter 2

## microphysics of neutron stars

### 2.1 equation of state of dense matter

The conditions in the interior of Neutron Stars are more extreme than any encountered terrestrially. The gravitational pressure is supported mainly by the pressure of the repulsive interaction of the nucleons. To a first approximation a neutron star is like a giant nucleus made of  $10^{57}$  nucleons (mostly neutrons) with an average baryon density close to the nuclear density. The star also has a solid *crust* roughly one kilometer thick, compositionally similar to terrestrial crystalline solids with highly neutron-rich nuclei. The **core** beneath the crust is essentially a sea of neutrons with a mere ten percent sprinkling of protons and an equal number of electrons to maintain charge neutrality. Besides having an average density of about  $\sim 10^{15} \text{ g cm}^{-3}$  a neutron star also has a huge neutron excess. When a neutron star forms in a supernova explosion the temperature attained is higher than the characteristic temperatures of all the equilibrating chemical reactions. Consequently, all of the neutron star material is  $\beta$ -equilibrated where most of the protons have been converted to neutrons due to enhanced inverse  $\beta$ -decay in a dense environment. As the electron Fermi sea is filled up the reverse process, i.e., the decay of a neutron to a proton, an electron and an anti-neutrino, is progressively blocked resulting in the neutron excess.

Except near the surface the neutron star behaves like an effective zero-temperature system, the actual temperature ( $\sim 10^6 \text{ K}$  or less in the crust and  $\lesssim 10^8 \text{ K}$  in the core after about  $10^4$  years) being much smaller than the characteristic temperatures (the Fermi temperature of the electrons or the neutrons or the energy of the nucleon-nucleon interaction). Therefore almost whole of the star can be described as a degenerate, free Fermi system (electrons being the dominant component near the surface and neutrons in the interior). We shall not discuss here the superfluid states of neutrons or protons

believed to exist in the core. Density-wise the neutron star has three characteristically different regions. The thin outer crust with densities ranging from  $10^6 \text{ g cm}^{-3}$  at the surface to  $4.0 \times 10^{11} \text{ g cm}^{-3}$  (neutron drip density) at which free neutrons start dripping out of the nuclei. Next is the inner crust with densities in-between the neutron-drip density and the nuclear density ( $2.8 \times 10^{14} \text{ g cm}^{-3}$ ). Beyond the nuclear density the nuclei dissolve to produce a soup of nucleons.

### 2.1.1 outer crust : $7.86 \text{ g cm}^{-3} < \rho < 4.0 \times 10^{11} \text{ g cm}^{-3}$

This is the best understood density regime of all. The pressure is primarily due to that of the degenerate electrons, charge neutrality being maintained by an ionic crystal. For  $\rho \gtrsim 10^6 \text{ g cm}^{-3}$  the electrons become relativistic. As density increases beyond this value the electron Fermi energy approaches the MeV range where it becomes energetically favourable for the protons to undergo inverse  $\beta$ -decay and convert themselves to neutrons giving rise to the neutron-rich nuclei in the crust. The equilibrium nuclide for a given density is obtained by minimizing the free energy of the system with respect to a particular combination of  $(Z, A)$  keeping the baryon number density constant. The first such calculation was done by Baym, Pethick & Sutherland (1971), reproduced here in table [2.1], based on Bethe-Weizsäcker semi-empirical mass formula with parameters obtained from fits to laboratory nuclei. Recently, Haensel, Zdunik & Dobaczewski (1989) have redone these calculations using more refined methods, though their results do not differ very much from the earlier ones. Among the factors important in deciding the equilibrium nuclide at a given density are the neutron and proton (dominant just below the neutron drip) shell effects and the strength of the spin-orbit interaction which depends on the three and higher body nucleon-nucleon interactions (defining the energy of the individual nuclei).

The pressure of a free, Fermi degenerate electron gas in the zero temperature phase is given by :

$$P_e = \frac{m_e c^2}{\lambda_e^3} \phi(x), \quad (2.1)$$

$$\phi(x) = \frac{1}{8\pi} \{x(1+x^2)^{1/2}(2x^2/3 - 1) + \ln[x + (1+x^2)^{1/2}]\}$$

where  $x$  ( $\frac{p_F}{m_e c}$ ) is the relativistic parameter and  $\lambda_e$  ( $\frac{\hbar}{m_e c}$ ) is the electron Compton wavelength. But the mass density is given by the rest-mass of the ions,

$$\rho = \mu_e m_u n_e = \frac{3}{\pi^2 \lambda_e^3} \mu_e m_u x^3, \quad (2.2)$$

where  $\mu_e$  is the mean molecular weight,  $m_u$  is the atomic mass unit and  $n_e \left( \frac{x^3}{3\pi^2 \lambda_e^3} \right)$  is the electron number density. To obtain the correct equation of state, several corrections have to be incorporated in the above expression for pressure. Firstly, the electrostatic correction arises because the positively charged ions are not uniformly distributed, but arranged in a crystal lattice with lattice sites having a charge  $Z$  each. This decreases the energy and the pressure of the ambient electrons as the distance between the repelling electrons is on an average larger than the mean distance between nuclei and electrons. Therefore, the repulsion is weaker than attraction. In a non-degenerate gas, the ratio between this Coulomb correction to the thermal energy is

$$\frac{E_c}{k_B T} \simeq \frac{Z e^2 / \langle r \rangle}{k_B T} \simeq Z e^2 n_e^{1/3} k_B T \quad (2.3)$$

and in a degenerate gas when Coulomb energy is comparable to the Fermi energy we have,

$$\frac{E_c}{E_F} \simeq c Z e^2 / \langle r \rangle p_F^2 / 2mc \simeq 2 \left( \frac{1}{3\pi^3} \right)^{2/3} \frac{Z}{a_0} \frac{1}{n_e^{1/3}} \quad , \quad (2.4)$$

where  $a_0 = \frac{\hbar^2}{m_e e^2}$  is the Bohr radius. When this correction is taken into consideration it is found that the pressure is modified as  $P = P_e - P_{\text{Coulomb}}$ , with  $P = 0$  for  $\rho = 7.86 \text{ g cm}^{-3}$ . Therefore, this is the minimum equilibrium density obtained at the very surface of the neutron star. At higher densities the most important correction is due to the inverse  $\beta$ -decay. The condition for the inverse  $\beta$ -decay ( $e^- + p \rightarrow n + \nu$ ) is that the kinetic energy of the electrons be larger than 1.24 MeV, the mass difference between a neutron and a proton. The  $\beta$ -decay of a neutron ( $n \rightarrow e^- + p + \nu$ ) is blocked when the density is so large that all the electron levels in the Fermi sea are filled up to the energy of the emitted electron.

The pressure is obtained by the thermodynamic relation  $P = n_B^2 \frac{\partial(\epsilon/n_B)}{\partial n_B}$ , where  $\epsilon$  is the total free-energy density including the rest-mass of the baryons and  $n_B$  is the baryon number density. When one species of nuclide changes to another as  $n_B$  changes there is a phase transition with an accompanying discontinuity in  $n_B$ . Since there can be no discontinuity in the pressure and the temperature inside the star to obtain the equilibrium composition and the equation of state Gibbs' free energy should be minimized. In this density range usually the equation of state obtained by Baym, Pethick & Sutherland (1971), incorporating the results of Feynman, Metropolis & Teller (1949) in the range  $7.9 \text{ g cm}^{-3} < \rho < 10^4 \text{ g cm}^{-3}$ , is used. In table [2.2] the equation of state (pressure vs. mass density) as calculated by them is shown.

TABLE 2.1

<i>DATA FROM BAYM, PETHICK AND SUTHERLAND (1971)</i>			
mass density	baryon number density	mass number of equilibrium nuclide	atomic number of equilibrium nuclide
$\rho$ (g cm <sup>-3</sup> )	$n_b$ (cm <sup>-3</sup> )	$Z$	$A$
7.8630	4.73324	26	56
7.9030	4.76324	26	56
8.15E0	4.91324	26	56
1.16301	6.99324	26	56
1.64301	9.90324	26	56
4.51301	2.72325	26	56
2.12302	1.27326	26	56
1.150E03	6.93326	26	56
1.044304	6.295327	26	56
2.622304	1.581328	26	56
6.587304	3.972328	26	56
1.654305	9.976328	26	56
4.156305	2.506329	26	56
1.044306	6.294329	26	56
2.622306	1.581330	26	56
6.588306	3.972330	26	56
8.293306	5.000330	28	62
1.655307	9.976330	28	62
3.302307	1.990331	28	62
6.589307	3.972331	28	62
1.315308	7.924331	28	62
2.624308	1.581332	28	62
3.304308	1.990332	28	64
5.237308	3.155332	28	64
8.301308	5.000332	28	64
1.045309	6.294332	28	64
1.316309	7.924332	34	84
1.657309	9.976332	34	84
2.626309	1.581333	34	84
4.164309	2.506333	34	84
6.601309	3.972333	34	84
8.312309	5.000333	32	82
1.046310	6.294333	32	82
1.318E10	7.924333	32	82
1.659310	9.976333	32	82
2.090310	1.256334	32	82
2.631310	1.581334	30	80
3.313310	1.990334	30	80
4.172310	2.506334	30	80
5.254310	3.155334	28	78

TABLE 2.1 (continued)

DATA FROM BAYM, PETHICK AND SUTHERLAND (1971)			
mass density	baryon number density	mass number of equilibrium nuclide	atomic number of equilibrium nuclide
$\rho$ (g cm <sup>-3</sup> )	$n_b$ (cm <sup>-3</sup> )	$Z$	
6.617E10	3.972E34	28	78
8.332E10	5.000E34	28	78
1.049E11	6.294E34	28	78
1.322E11	7.924E34	28	78
1.664E11	9.976E34	26	76
1.844E11	1.105E35	42	124
2.096E11	1.256E35	40	122
2.640E11	1.581E35	40	122
3.325E11	1.990E35	38	120
4.188E11	2.506E35	36	118
4.299E11	2.572E35	36	118
4.460E11	2.670E35	40	126
5.228E11	3.126E35	40	128
6.610E11	3.951E35	40	130
7.964E11	4.759E35	41	132
9.728E11	5.812E35	41	135
1.196E12	7.143E35	42	137
1.471E12	8.786E35	42	140
1.805E12	1.077E36	43	142
2.202E12	1.314E36	43	146
2.930E12	1.748E36	44	151
3.833E12	2.287E36	45	156
4.933E12	2.942E36	46	163
6.482E12	3.726E36	48	170
7.801E12	4.650E36	49	178
9.611E12	5.728E36	50	186
1.246E13	7.424E36	52	200
1.496E13	8.907E36	54	211
1.778E13	1.059E37	56	223
2.210E13	1.315E37	58	241
2.988E13	1.777E37	63	275
3.767E13	2.239E37	67	311
5.081E13	3.017E37	74	375
6.193E13	3.675E37	79	435
7.732E13	4.585E37	88	529
9.826E13	5.821E37	100	683
1.262E14	7.468E37	117	947
1.586E14	9.371E37	143	1390
2.004E14	1.182E38	201	2500
2.004E14	1.182E38	201	2500

TABLE - 2.2

<i>EQUATION OF STATE FROM BAYM, PETHICK AND SUTHERLAND (1971)</i>			
mass density	pressure	mass density	pressure
$\rho$ (g cm <sup>-3</sup> )	P (dyne cm <sup>-2</sup> )	$\rho$ (g cm <sup>-3</sup> )	P (dyne cm <sup>-2</sup> )
7.8630	1.01309	1.316309	5.036326
7.9030	1.01310	1.657309	6.860326
8.1530	1.01311	2.626309	1.272327
1.16301	1.21312	4.164309	2.356327
1.64301	1.40313	6.601309	4.362327
4.51301	1.70314	1.046310	7.702327
2.12302	5.82315	8.312309	5.662E27
1.150303	1.90317	1.318310	1.048328
1.044304	9.744318	1.659310	1.425328
2.622304	4.968319	2.090310	1.938328
6.587304	2.431320	2.631310	2.503328
1.654305	1.151321	3.313310	3.404328
4.156305	5.266321	4.172310	4.628328
1.044306	2.318322	5.254310	5.949328
2.622306	9.755322	6.617310	8.089328
6.588306	3.911323	8.332310	1.100329
8.293306	5.259323	1.049311	1.495329
1.655307	1.435324	1.322311	2.033329
3.302307	3.833324	1.664311	2.597329
6.589307	1.006325	1.844311	2.892329
1.315308	2.604325	2.096311	3.290329
2.624308	6.676325	2.640311	4.473329
3.304308	8.738325	3.325311	5.816329
5.237308	1.629326	4.188311	7.538329
4.299311	7.805329	8.301308	3.029326
1.045309	4.129326		

### 2.1.2 inner crust : $4.0 \times 10^{11} \text{ g cm}^{-3} < \rho < 2.8 \times 10^{14} \text{ g cm}^{-3}$

At the lower edge of this regime, the neutron energy levels within the nuclei merge into a continuum and they drip out of the nuclei to comprise a free neutron gas co-existing with the crystal lattice of the neutron-rich nuclei. The problem of calculating an accurate equation of state here is that the correct nucleon-nucleon potential is not known to any degree of certainty, and that the quantum many-body techniques are not quite adequate to solve the Schrodinger equation given the potential. In this regime, with the proton-to-neutron ratio ranging from 0.1 to 0.3, extrapolations based on semi-empirical

## DOMINANT 2-BODY INTERACTION BY PION EXCHANGE

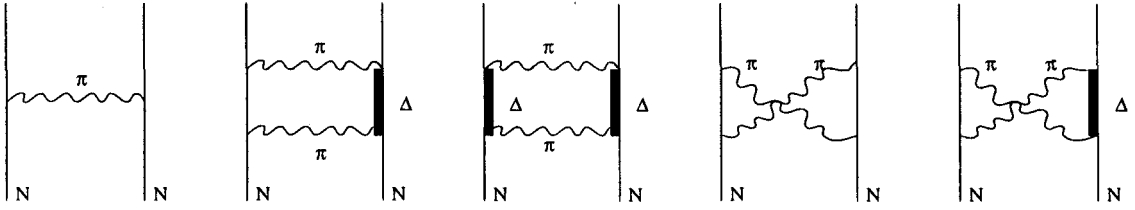


Figure 2.1: Feynman diagrams showing two-nucleon interaction by exchange of pions. The single lines, the wavy lines and the thick lines stand for the world lines of the nucleons, the pions and the virtual  $\Delta$  particles respectively.

mass formula is used. The work done by Baym, Bethe & Pethick (1971) took care of the fact that the neutrons inside and outside the nuclei behave in a similar fashion. The nuclear surface energy is modified by the free neutron gas outside. By using a *compressible liquid drop model* of nuclei they minimized the total energy, for a fixed value of the baryon density  $n_B$ , for an equilibrium configuration. Free neutrons supply an increasingly larger fraction of the pressure as the density increases.

But these earlier works did not take the nuclear shell effects into account, as was later done by Negele & Vautherin (1973). The main feature of this work has been the modeling of the nucleon-nucleon interaction by taking into consideration the two-body interactions only. The dominant two-body interaction, by exchange of pions, come from processes like the ones in figure [2.1]. The equation of state in the above mentioned density range is given by the following interpolation formula :

$$E_t = m_n + \sum_{i=0}^7 c_i x^{i-1} \quad (2.5)$$

$$\rho = \frac{n_b E_T}{c^2} \quad (2.6)$$

$$P = n_b^2 \frac{\partial E_T}{\partial n_b} \quad (2.7)$$

where  $m_n$  is the mass of the neutron and  $x = \ln(n_b \times 10^{-35})$ ,  $n_b$  being the baryon number density. The constants  $c_i$ s are given in table [2.3].

Another important fact is that at these densities the solid state and the nuclear energies are comparable. Hence they require to be treated on equal footing. This leads to the possibility of existence of non-spherical nuclei. It has been shown by Lorenz, Ravenhall & Pethick (1993) that at sub-nuclear densities nuclei with rod or disc shape are likely to exist. If they indeed do, that will introduce a modification in the equation

of state in these density ranges and may in turn affect the structure and other physical properties (like the transport coefficients or the thermal evolution) of a neutron star.

TABLE - 2.3

<i>COEFFICIENTS FOR CALCULATION OF THE EQUATION OF STATE FROM NEGELE AND VAUTHERIN (1973)</i>	
<b>i</b>	<b>c<sub>i</sub> (ground state)</b>
<b>0</b>	<b>-4.0</b>
<b>1</b>	<b>2.8822899 x 10<sup>-1</sup></b>
<b>2</b>	<b>5.9150523 x 10<sup>-1</sup></b>
<b>3</b>	<b>9.0185940 x 10<sup>-2</sup></b>
<b>4</b>	<b>-1.1025614 x 10<sup>-1</sup></b>
<b>5</b>	<b>2.9377479 x 10<sup>-2</sup></b>
<b>6</b>	<b>-3.2618465 x 10<sup>-3</sup></b>
<b>7</b>	<b>1.3543555 x 10<sup>-4</sup></b>

### 2.1.3 the core : $\rho > 2.8 \times 10^{14} \text{ g cm}^{-3}$

The theories at these densities are faced with a plethora of problems. There is a lack of understanding of the correct form for the nucleon-nucleon potential added to the fact that there is no laboratory data available to test the theory against. As the density increases the effects of relativity becomes important. Also at higher densities it is essential to incorporate the non-nucleonic degrees of freedom as mesons and higher mass baryons make appearance. At extreme high densities there may probably occur a phase transition to the quark phase and then quark and gluonic degrees of freedom should also have to be taken into account. And even at nuclear saturation densities the predictions regarding the possible phase transition to a superfluid/superconducting phase are not without uncertainties. One of the major problems in trying to understand the nuclear phenomena inside a neutron star is due to the huge neutron excess. The parameter  $\delta = (N - Z)/(N + Z)$ , used to denote the neutron excess is about 1/4 in terrestrial nuclei. In neutron stars, starting from that value at the surface  $\delta$  becomes as large as unity deep in the interior of the star. Any extrapolation, that requires going up by a factor of four, is bound to be unreliable.

Nevertheless, we have reasonable estimates for the nucleon-nucleon interaction based

## DOMINANT 3-BODY INTERACTION BY PION EXCHANGE

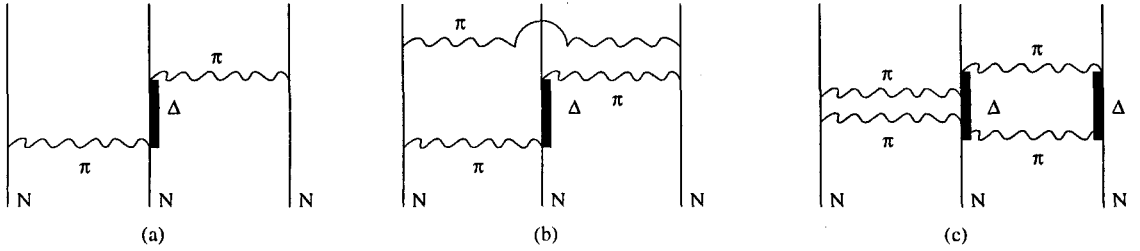


Figure 2.2: Feynman diagrams showing three-nucleon interaction by exchange of pions. The single lines, the wavy lines and the thick lines stand for the world lines of the nucleons, the pions and the virtual  $\Delta$  particles respectively.

on the scattering data from the laboratory experiments. But these provide information only about the long-range behaviour of the potential. There is no handle on the **short-range** behaviour, which is likely to dominate at the neutron star densities. From the data on the binding energy of light nuclei the microscopic Hamiltonian is modelled. But aspects of interaction that are relatively unimportant for such light nuclei (deuterium,  $\text{He}^3$  etc.) may play significant roles in a neutron star. Of particular importance are the three and higher body interactions. At long range, the most important three-body interaction is that due to the exchange of pions, where one of the nucleons becomes converted to a  $\Delta$  and then de-excites back by exchanging another pion with a third nucleon (figure [2.2a]). At short-range other processes like those in figures [2.2b] and [2.2c] dominate.

To summarize, we mention the three equations of state which incorporate some of the recent developments, following Wiringa, Fiks & Fabrocini (1988) (though more recent calculations for the equation of state in this density range has been performed, see for example Prakash et al. 1992). In this paper, they compare the equations of state obtained by using different types of two-body and three-body potentials as against the equation of state for a pure, free neutron gas. The two-body potentials used by them are AV14 (Argonne 14) and UV14 (Urbana 14) both of which fit the scattering data well but differ in their short-range behaviour. These are modified with the three-body interaction UVII which is adjusted to fit the binding energies of  $\text{He}^3$  and  $\text{He}^4$ . The other three-body interaction TNI is less complete in taking into account all aspects of the three-body interaction. It is observed that, at  $\rho \sim 3 - 4\rho_s$ , where  $\rho_s$  is the saturation nuclear density, the total energy per particle differs by an amount small compared

to the mass of the neutrons from that obtained by using a free-neutron gas. It is also seen that the energy per particle depends on the choice of the two-body as well as the three-body interaction. Lastly, though the energy does not change much, the pressure, given by the slope of the energy curve ( $P(\rho) \sim \frac{\partial E(\rho)}{\partial \rho}$ ), is very different for different equations of state. In table [2.4], is the data from Wiringa, Fiks & Fabrocini (1988) for the three equations of state.

TABLE - 2.4

<i>DATA FROM WIRINGA, FIKS AND FABROCINI (1971)</i>						
	AV14 + UVII		UV14+UVII		UV14+TNI	
mass density $\rho$	proton fraction $x(\rho)$	energy density $E(\rho, x)$	proton fraction $x(\rho)$	energy density $E(\rho, x)$	proton fraction $x(\rho)$	energy density $E(\rho, x)$
$fm^{-3}$		Mev/nucleon		Mev/nucleon		Mev/nucleon
0.07	0.017	7.35	0.019	8.13	0.026	5.95
0.08	0.019	7.94	0.021	8.66	0.029	6.06
0.10	0.023	8.97	0.025	9.79	0.033	6.40
0.125	0.027	10.18	0.030	11.06	0.037	7.17
0.15	0.031	11.43	0.035	12.59	0.042	8.27
0.175	0.036	12.74	0.042	14.18	0.047	9.70
0.20	0.044	14.12	0.052	15.92	0.051	11.55
0.25	0.051	16.96	0.069	20.25	0.057	16.29
0.30	0.051	20.48	0.079	25.78	0.059	22.19
0.35	0.052	24.98	0.087	32.60	0.060	28.94
0.40	0.055	30.44	0.097	40.72	0.060	36.60
0.50	0.060	45.15	0.116	61.95	0.051	56.00
0.60	0.077	66.40	0.132	90.20	0.039	79.20
0.70	0.099	93.60	0.155	126.20	0.023	106.10
0.80	0.101	132.10	0.172	170.50	0.005	135.50
1.00	0.094	233.00	0.177	291.10	0.0009	200.9
1.25	0.066	410.00	0.122	501.00	0.00	294.00
1.50	0.014	635.00	0.026	753.00	0.00	393.00

A combination of the Baym, Pethick & Sutherland (BPS), Negele & Vautherin (NV) and Wiringa, Fiks & Fabrocini (WFF) equations of state in the respective density ranges seem to be the most acceptable considering all the uncertainties mentioned

above. In our subsequent calculation of the structure of a neutron star we shall use this combination as our starting point. Amongst the three equations of state given by Wiringa et al. we have used only the second one mentioned as UV14+UVII in the discussion above.

## 2.2 mass and density profile of a neutron star

In this thesis we investigate the temporal behaviour of the magnetic fields assuming a crustal current. This requires an accurate knowledge of the various transport coefficients (most importantly thermal and electrical conductivity) in the crust. Therefore, we need an accurate density profile, particularly in the low density crustal regions, to obtain the radial behaviour of the transport coefficients. The mass and density profiles for a non-rotating, self-gravitating object are obtained by integrating the hydrostatic pressure balance equation

$$\frac{dP(r)}{dr} = -\frac{GM(r)\rho(r)}{r^2}, \quad (2.8)$$

along with the equation of mass distribution,

$$\frac{dM(r)}{dr} = 4\pi r^2 \rho(r), \quad (2.9)$$

where  $P(r)$ ,  $M(r)$  and  $\rho(r)$  are the pressure, mass and density at a given radius  $r$  and  $G$  is the gravitational constant. Equation [2.8] is modified, when effects of general relativity is incorporated, to :

$$\frac{dP(r)}{dr} = -\frac{G(M(r) + 4\pi r^3 P(r)/c^2)(\rho(r) + P(r)/c^2)}{r^2(1 - \frac{2GM(r)}{r^2 c^2})}, \quad (2.10)$$

where  $c$  is the speed of light. This is known as the TOV equation after Tolman, Oppenheimer and Volkoff (Oppenheimer & Volkoff, 1939). A measure of the importance of general relativity is given by the quantity  $\epsilon \sim \frac{GM}{Rc^2}$  for a self-gravitating body of rest mass  $M$  and total radius  $R$ . For  $\epsilon \ll 1$ , the effect of relativity can be neglected. Putting in the typical numbers for a neutron star we obtain  $\epsilon$  to be close to 1. Therefore, to obtain the mass-density profile of a neutron star it is required to solve the TOV equation instead of the Newtonian hydrostatic equation. We solve equations [2.9] and [2.10] numerically. The equation of state we use for this structure calculation is of moderate stiffness and is given by Baym, Pethick & Sutherland (1971) in the density range  $10^6 \text{ g cm}^{-3} < \rho < 4.0 \times 10^{11} \text{ g cm}^{-3}$ , by Negele & Vautherin (1973) in the range  $4.0 \times 10^{11} \text{ g cm}^{-3} < \rho < 2.8 \times 10^{14} \text{ g cm}^{-3}$ , and by Wiringa, Fiks & Fabrocini (1988) in the range  $2.8 \times 10^{14} \text{ g cm}^{-3} < \rho$ . In figures [2.3], [2.4], [2.5] - the pressure vs. density

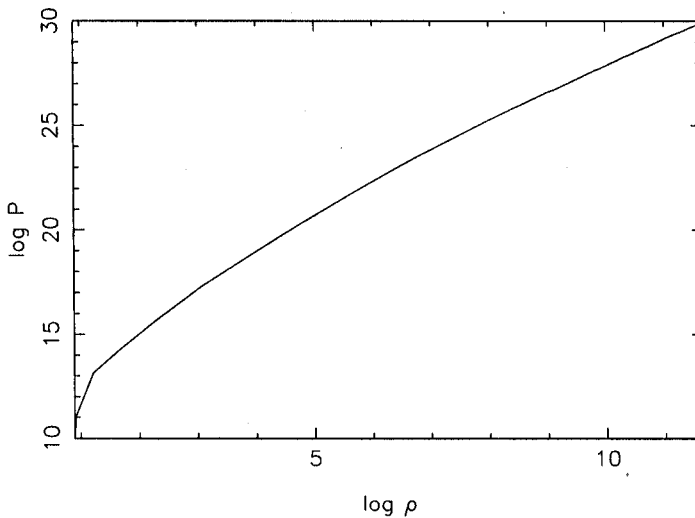


Figure 2.3: Pressure vs. Density from Baym, Pethick & Sutherland (1971)

as obtained in these three ranges have been plotted.

Though the structure calculations have been performed by many people (see for example Wiringa, Fiks & Fabrocini 1988) an accurate density profile in the low density regime of the crust, has been lacking. Therefore, we undertook the task of obtaining the density profile for a typical neutron star, by integrating the TOV equation, using above-mentioned equations of state. It must be mentioned here that in a recent work Datta, Thampan & Bhattacharya (1995) have performed detailed calculations of the crustal density profile of neutron stars for a number of equations of state. One ought to note that the equations of state for different density regimes are not exactly matched at the boundaries. So we use a smoothing procedure ensuring the continuity of the pressure and the pressure gradient at each boundary. This smoothed composite equation of state is plotted in figure [2.6].

We integrate the TOV equation starting from a particular central density and corresponding central pressure at zero radius. The other boundary condition at the centre is that of zero mass. The set of coupled second order ordinary differential equations are solved using a fourth order Runge-Kutta scheme of differencing. We have used the ordinary differential equation solver programs by Press et. al (1992) for the Runge-Kutta driver with an adaptive step-size control. The adaptive step-size control is essential

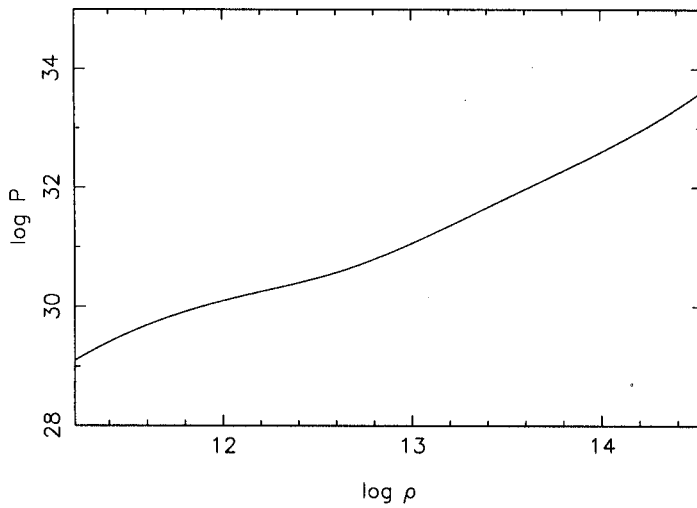


Figure 2.4: Pressure vs. Density from Negele & Vautherin (1973).

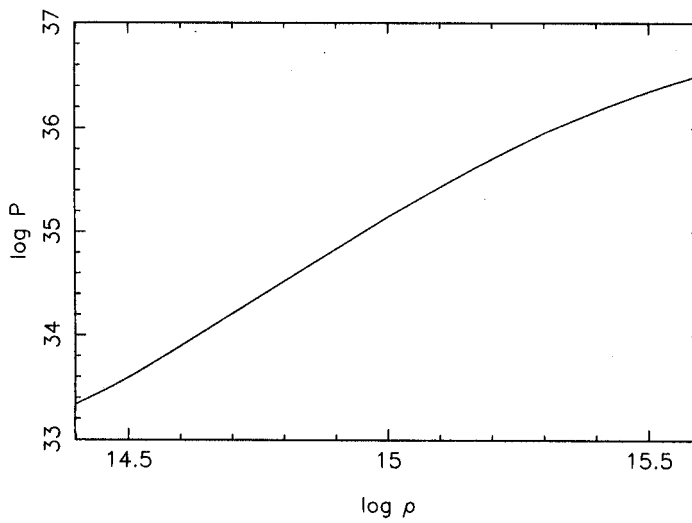


Figure 2.5: Pressure vs. Density from Wiringa, Fiks & Fabrocini (1988).

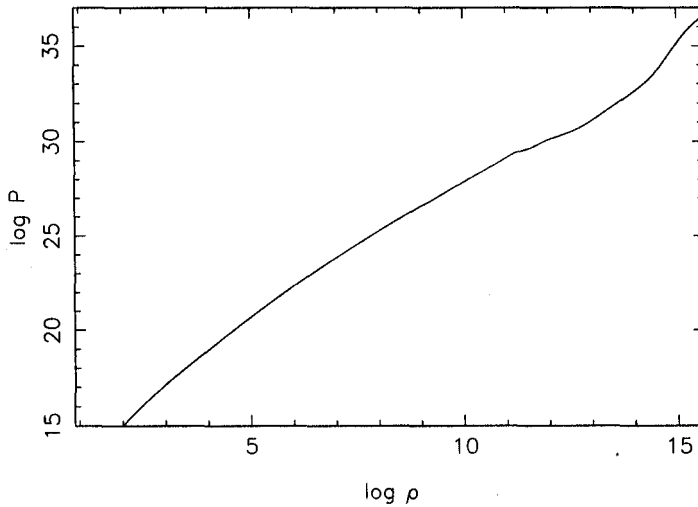


Figure 2.6: Pressure vs. Density : Smoothed out over the whole density range.

in integrating the mass-density profile since both the functions show extremely steep behaviour near the surface, at the low density regime. In our computation the surface corresponds to a density of  $7.86 \text{ g cm}^{-3}$  as that is the minimum density obtained in the neutron star. The density and the mass profiles for a neutron star of total mass  $1.4M_{\odot}$  are plotted in figures [2.7] and [2.8] respectively.

For different central densities, the total mass and the radius of the star differ quite a lot. The variation of the total mass and the radius with central density have been plotted in figures [2.9] and [2.10]. And the mass-radius relation for a set of neutron stars state is plotted in figure [2.11]. This clearly shows the existence of a maximum mass, which could also be seen (albeit with some difficulty) in figure [2.9]. This maximum mass of about  $2.2 M_{\odot}$  corresponds to a central density of  $\sim 2.5 \times 10^{15} \text{ g cm}^{-3}$  and a radius of 10 km.

We plot the variation of the mass of the overlying layers and density with the depth from the surface in figures [2.12] and [2.13]. It should be noted that the density changes sharply with depth whereas the mass remains almost constant close to the surface and then shows a sharp increase. This is due to the fact that the mass in the outer layers of the neutron star is very small. In figure [2.14] we have plotted the mass of the core and the mass of the crust as functions of the total mass. It is seen that with an increase in

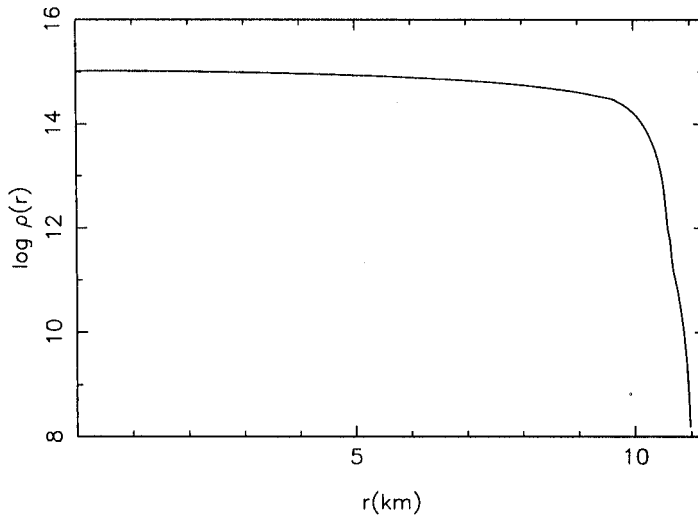


Figure 2.7: Density vs. Radius for a  $1.4 M_{\odot}$  neutron star.

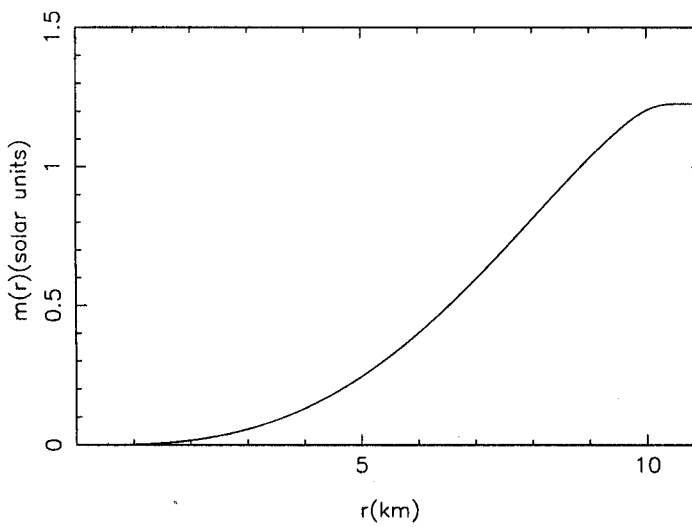


Figure 2.8: Mass vs. Radius for a  $1.4 M_{\odot}$  neutron star.

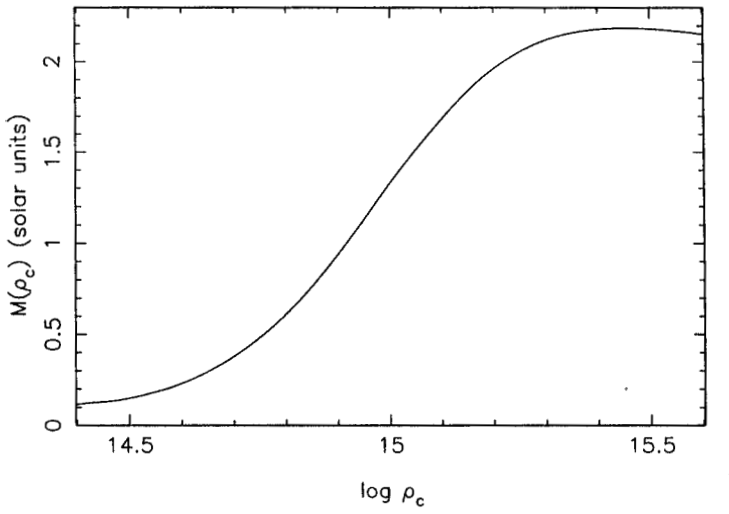


Figure 2.9: Total Mass vs. Central Density

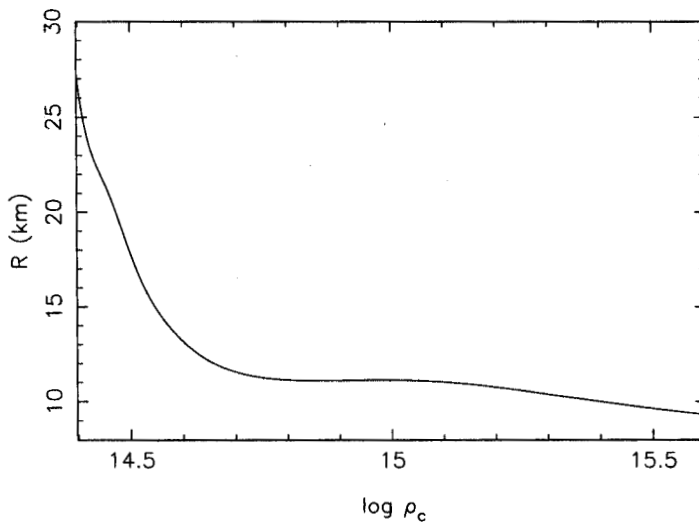


Figure 2.10: Stellar Radius vs. Central Density

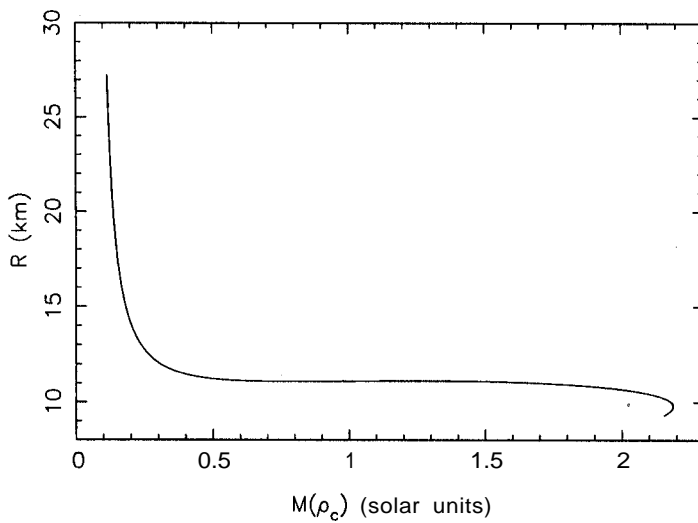
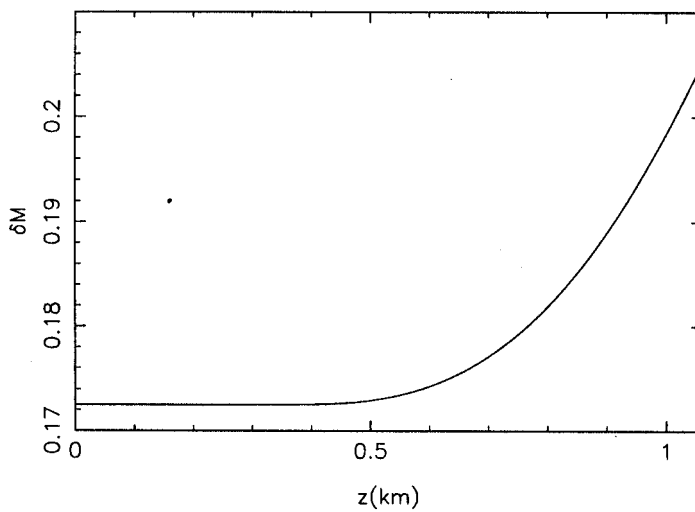


Figure 2.11: Stellar Radius vs. Total Mass

Figure 2.12: Mass (in solar units) of the overlying layers vs. Depth (from the surface) of the layer in a  $1.4 M_{\odot}$  neutron star.

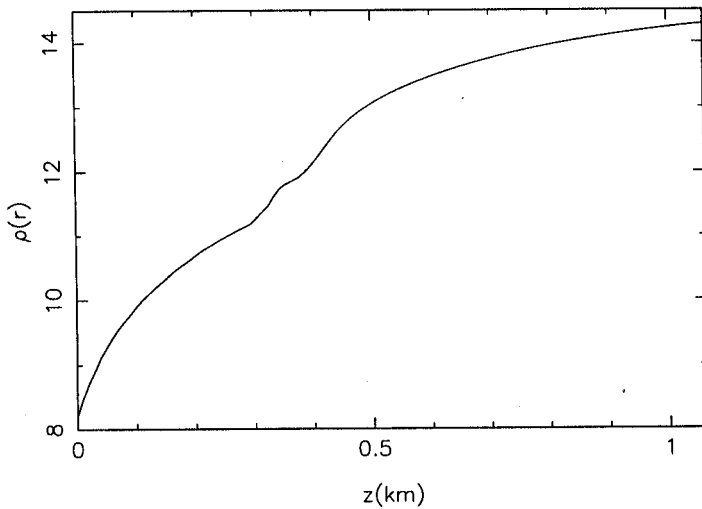


Figure 2.13: Density vs. Depth (from the surface) a  $1.4 M_{\odot}$  neutron star.

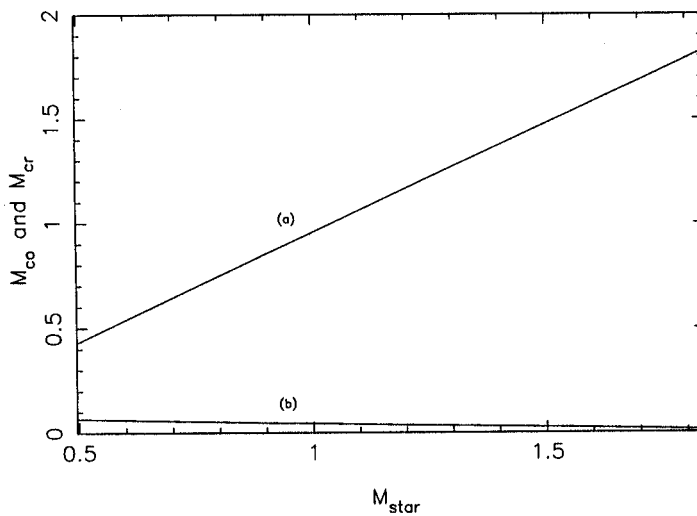


Figure 2.14: Variation of the core-mass and the crust-mass with the total mass of a neutron star. Curves (a) and (b) refer to the core and crust mass respectively.

RAMAN RESEARCH INSTITUTE  
BANGALORE-80

CLASS No. .... 043; 524.354.6 SVS

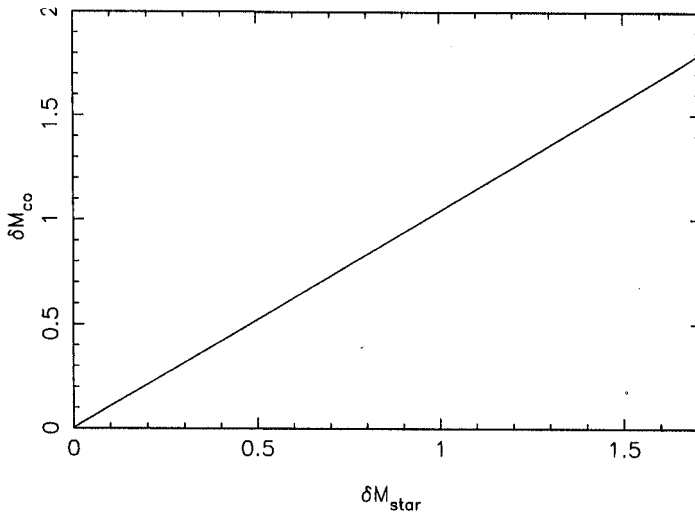


Figure 2.15: Variation of the change in the core-mass with a change in the total mass of a neutron star.

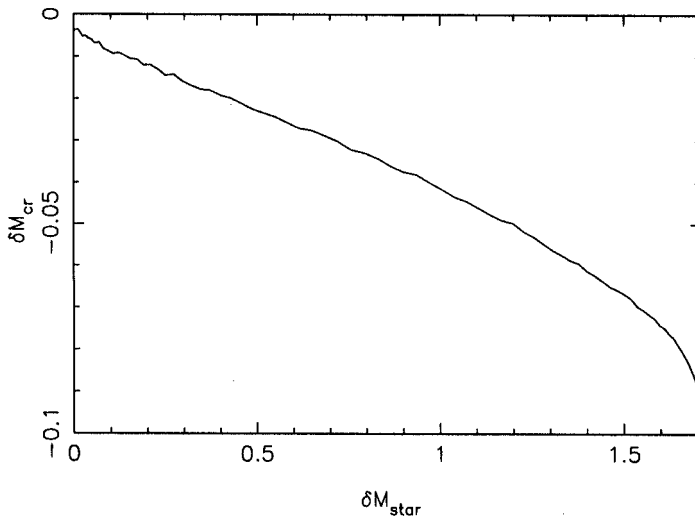


Figure 2.16: Variation of the change in the crust-mass with a change in the total mass of a neutron star.

the total mass the mass of the core increases almost by the same amount. Whereas, the change in the mass of the crust is minimal. Figures [2.15] and [2.16] in which we plot the change in crustal and core mass vs. a change in the total mass brings this fact out more dramatically.

## 2.3 thermal evolution of neutron stars

### 2.3.1 isolated neutron star

Thermal evolution of a system is determined by the processes of energy loss and those of heat generation. In the case of a neutron star heat loss is mainly by emission of neutrinos from the interior and by emission of photons from the surface of the star. There are various mechanisms for internal heat generation, for example, friction due to differential rotation of crustal neutron superfluid, dissipative processes due to the core proton superconductor, heat release by chemical change in the crust induced by spin-down of the star, ohmic dissipation of current loops (supporting the magnetic field) due to the finite conductivity in the crust or crust cracking etc (for details of neutron star thermal evolution see Lattimer et al. 1991, Pethick 1992, Page 1997 and references therein).

The dominant mechanism of cooling in the early phases of thermal evolution is that of neutrino emission. Different regions of the star produce neutrinos by different mechanisms, namely, by **URCA** process in the core and neutrino pair bremsstrahlung in the crust. The comparability of the two processes depends on the presence of exotic phases in the core and whether direct **URCA** process can proceed in the core after it has cooled down below  $\sim 10^{11}$  K. It also depends on the band-structure of the electrons in the crust of the star, which may suppress the neutrino pair bremsstrahlung considerably. In the core, if the matter is a normal n-p-e plasma and the proton fraction is not too high then neutrinos are emitted via modified **URCA** process. Through this process the star cools with a time-scale of  $T^{-8}$ . In presence of exotic phases like quark matter or Bose condensates of kaons or pions direct **URCA** process can proceed. With a  $T^{-6}$  dependence on temperature this process results in rapid cooling. Since the state of the matter in the core of a neutron star is not known with any certainty, there is a lot of controversy about whether direct or modified **URCA** processes control neutron star thermal evolution. Moreover, there is uncertainty in the rate calculation for the modified **URCA** process due to medium effects etc and therefore a comparison with observation does not yet provide a definite answer.

All of the above discussion assumes the matter to be normal and the spectrum of elementary excitations smooth near the Fermi surfaces of the particles. In presence of superfluidity or superconductivity gaps would open up near the Fermi surfaces suppressing neutrino emission at temperatures less than the gap energy. Under these conditions the neutrino pair bremsstrahlung is the dominant cooling process. Recent work by Pethick & Thorsson (1994) has shown that this crust cooling process may get suppressed due to the creation of the band structure as electrons move in the periodic lattice potential, below a temperature of  $10^{10}$ K. Recently, the effect of Cooper pair breaking and formation has also been incorporated in the thermal evolution calculations (Schaab et al. 1997).

In a recent work Iwamoto et al. (1995) have shown that a finite magnetic moment of neutrino would significantly modify the cooling history of a neutron star in the very early phases. This makes the crustal cooling compete with the core cooling within the typical time scale that conduction takes to transport thermal energy from the core to the surface.

It appears that the present data is compatible with both the slow and fast cooling processes (modified and direct URCA) as there is a lot of uncertainty in all the mechanisms involved in the thermal evolution of a neutron star. In figure [2.17] taken from Page (1997) different theoretical scenarios could be seen and how these theories compare with the observational values of surface temperatures measured for various pulsars. There are other factors that may be responsible for a discrepancy between the theory of the thermal evolution of the neutron stars and the observed values for the surface temperatures. For example the temperature is usually estimated assuming the neutron star to behave like a perfect black-body, but the pressure of an atmosphere and the effects of a strong magnetic field may significantly modify this result (Pavlov, Zavlin, Trümper & Neuhauser 1996, Shibunov & Yakovlev, 1996).

### 2.3.2 thermal structure of an isolated neutron star

Temperature fluctuations in the interior of the neutron star are smoothed out very fast due to its large thermal conductivity and effectively the whole of the star behaves like an isothermal system, except at the layers close to the surface (Gudmundsson, Pethick & Epstein 1982). Though the temperature of the entire region beyond a density of  $10^{10}$  g cm<sup>-3</sup> is practically the same, it drops by almost two orders of magnitude at the

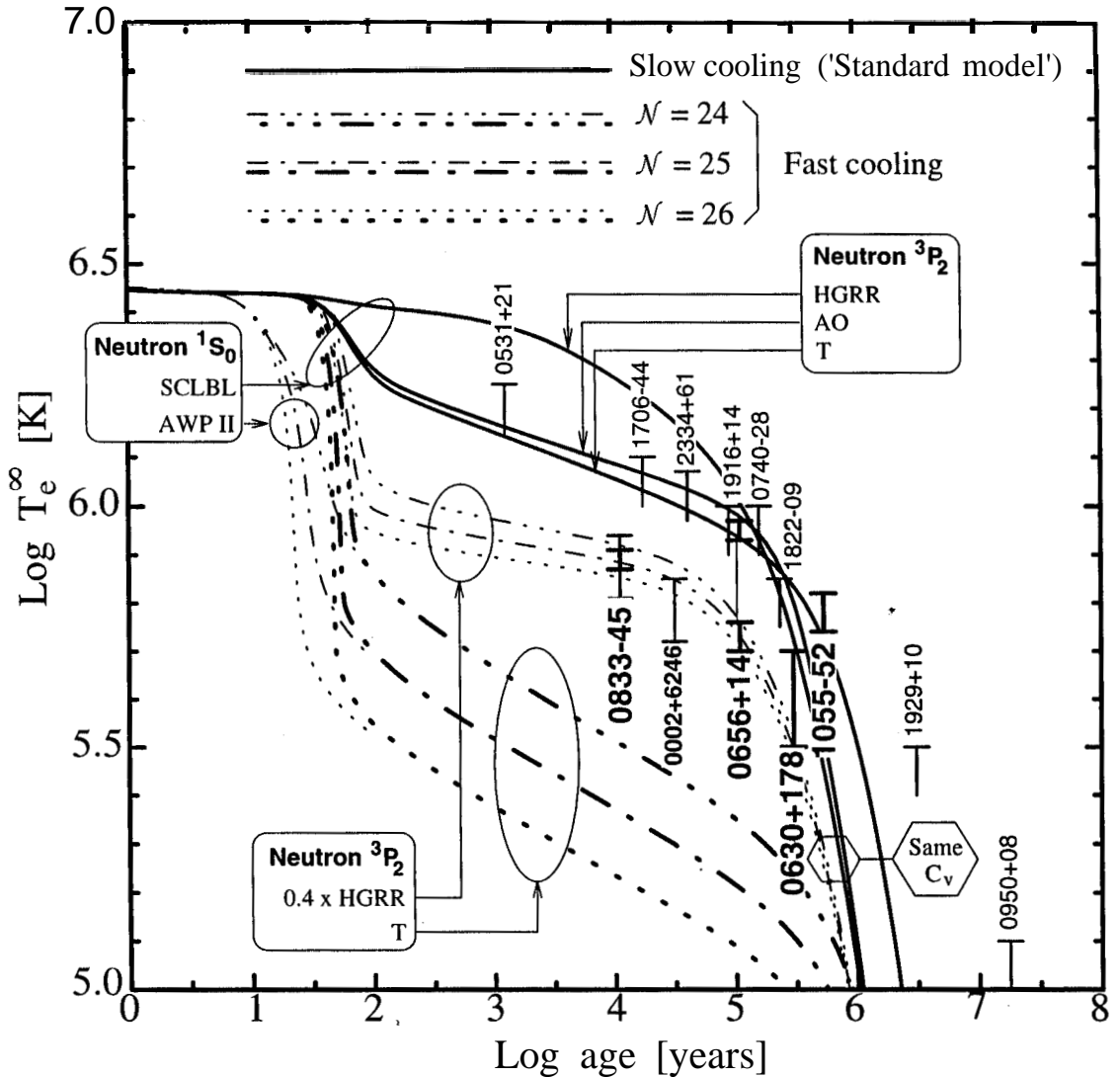


Figure 2.17: **Typical behavior of slow ('standard') and fast cooling scenarios.**  $1.4 M_{\odot}$  neutron stars with the Friedman & Pandharipande (1981) equation of state. The cases with  $\mathcal{N} = 24, 25,$  and  $26$  correspond approximately to the effect of a kaon condensate, pion condensate, and the direct URCA process (with hyperons or nucleons), respectively. The various curves, within each scenario, show the effect of various assumptions about pairing: all models use the proton  $^1S_0$   $T_c$  'T', and the neutron  $^1S_0$  and  $^3P_2$   $T_c$ 's are as labeled. All models have non-magnetized iron envelopes. Neither Cooper pair breaking and formation neutrino emission nor heating are included. The main effect of pairing in the crust (neutron  $^1S_0$ ) is to shorten the length of the early plateau. Core pairing suppresses the neutrino emission, which results in a higher  $T_e$  during the neutrino cooling era (age from  $\sim 100$  to  $\sim 10^5$  yr), and the specific heat, which results in faster cooling during the photon cooling era (age above  $\sim 10^5$  yr). The reduction of the specific heat during the neutrino cooling era does not show up as much as during the photon cooling era due to the small slope of the curves at this phase. All points are really upper limits (in several cases based on a non-detection of the pulsar) but for the radio pulsars 0833–45 (Vela), 0656+14, 0630+178 (Geminga), 1055–52, and the neutron star 0002+6246, there is good evidence that the observed X-rays are from surface thermal emission. Uncertainty on the temperature estimate is illustrated in the case of PSR 0656+14 where two values are reported. (from Page, 1997)

outermost layers of the star. The work of Gudmundsson, Pethick & Epstein (1982, 1983) on the envelopes of non-magnetic neutron stars showed that the temperature of the isothermal interior,  $T_b$ , depends only on the surface temperature and the surface gravity of the star :

$$T_b = 1.288 \times 10^8 K \left( \frac{(T_s/10^6 K)^4}{g_s/10^{14} \text{cms}^{-2}} \right)^{0.455} \quad (2.11)$$

where  $T_s$  is the surface temperature and  $g_s$  is the surface gravity. These authors also present the variation of the temperature with density between the surface and the isothermal interior. To obtain temperature as a function of density in these outer regions of the crust we use the following fitting formula to their plots :

$$T(\rho) = \left( \frac{\rho}{\rho_{\text{boundary}}} \right)^{1/4} T_b, \quad \rho \leq \rho_{\text{boundary}} \quad (2.12)$$

where  $\rho_{\text{boundary}}$  is the density beyond which the temperature stays effectively constant.

### 2.3.3 accreting neutron star

The thermal history of an accreting neutron star is very different from that of an isolated one. The cooling of an isolated neutron star brings the surface temperature down to  $\sim 10^{4.5}$  K in about  $10^7$  yr (van Riper 1991a, b) with an attendant interior temperature of the nearly isothermal core of the order of  $10^7$  K. Therefore when mass accretion starts this cold star is heated up due to the entropy inflow of the accreted matter. The temperature rise might be enough to start nuclear burning at the surface and one expects pycnonuclear shell burning of hydrogen and helium. Within a short time ( $\sim 10^5$  yr) almost the entire crust is heated to a constant temperature of the order of  $10^{7.5} - 10^{8.5}$  K (Miralda-Escudé, Haensel & Paczyński 1990). This is ignoring an initial short phase in which both the rate of accretion and the temperature of the crust show time evolution. The rate of accretion stabilizes in a few thousand years (Savonije 1978). The temperature that the crust will finally attain in the steady phase has been computed by Fujimoto et al. (1984), Miralda-Escudé et al. (1990) and Zdunik et al. (1992). However, these computations are restricted to limited range of mass accretion and also do not yield the same crustal temperature under similar conditions. The results obtained by Zdunik et al. (1992) for the crustal temperatures for a given accretion rate in the range  $10^{-15} M_{\odot}/\text{yr} < \dot{M} < 2 \times 10^{-10} M_{\odot}/\text{yr}$  could be fitted to the following formula:

$$\log T = 0.397 \log \dot{M} + 12.35. \quad (2.13)$$

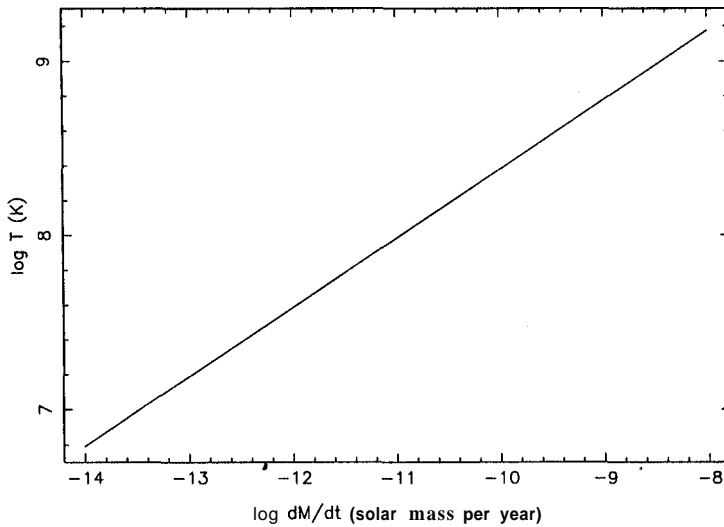


Figure 2.18: Variation of the constant isothermal temperature of the crust of a neutron star with accretion rate.

But extrapolation of this fit to higher rates of accretion gives extremely high temperatures which would not be sustainable for any reasonable period due to rapid cooling by neutrinos at those temperatures. For the purpose of our calculations, we use equation [2.13] as long as the temperature of the crust is smaller than  $10^{8.5}$  K. Beyond that we freeze the temperature at that upper limit. In figure [2.18] we have plotted the variation of the crustal temperature with accretion rate according to equation [2.13]. The thermal state of the core depends strongly on the neutrino emissivity whereas the crust remains largely indifferent to that. The core stays relatively cool if there is pion condensate inside which induces enhanced neutrino cooling, otherwise the core temperature may also be raised to a large extent by mass accretion.

The above discussion does not take into account the fact that the composition of the accreted layers could be very different from that of the original cold catalysed composition. In a recent work it has been shown that the presence of light elements in the accreted envelope enhances the emission processes in the photon cooling era and hence ultimately a faster cooling rate is achieved (Chabrier, Potekhin & Yakovlev 1997). Such effects show drastic difference in the surface temperature (see Page 1997 for a discussion) already within ten thousand years. If incorporated, this might change the evolution of the magnetic field considerably.

## 2.4 transport properties in the crust of neutron stars

The investigations of the transport properties of ultra-dense matter arise out of the interest in the evolution of the thermal state and the magnetic field in white dwarfs and neutron star crusts. See Itoh (1994) and references therein for a good review on the transport properties of neutron star crust. It has already been mentioned in section [2.1] that the crust of a neutron star consists of a relativistic, Fermi-degenerate free electron gas plus a non-relativistic, non-degenerate liquid/crystal of ions. It is assumed that the material is completely pressure-ionized. The density at which this happens is given by the condition

$$\rho \geq 0.378AZ^2 \text{ g cm}^{-3}, \quad (2.14)$$

which turns out to be  $\sim 10^4 \text{ g cm}^{-3}$  for  $\text{Fe}^{56}$  ions. Therefore, the lower boundary for which the transport properties have been worked out is this particular density. Though, recently, Itoh, Hayashi & Kohyama (1993) have investigated the entire density range below this value.

The thermal and electrical conduction is basically carried out by the electrons. The electrical conductivity is given by following simple Drude formula (Ashcroft & Mermin 1976)

$$\sigma = \frac{n_e e^2 \tau}{m_*}, \quad (2.15)$$

where  $n_e$  is the number density of electrons and  $m_*$  is the effective mass of the electron in the crystal.  $\tau$  is the time-scale of the collision of electrons with the ions (in liquid phase) or **phonons/impurities** (in case of a crystalline solid). It must be mentioned here that although the importance of quantum corrections have been realized in the present context, not much progress has been made in that direction.

In the crust of a neutron star both density and temperature vary with radius. Whereas the uppermost layers close to the surface are likely to be in a liquid state, the inner crust is a crystalline solid. The condition for **melting/crystallization** of a classical one-component plasma is given by Lindeman criterion. According to this criterion (Slattery, Doolen & Dewitt, 1982)

$$\Gamma = \frac{\text{Coulomb Energy of the Crystal}}{\text{Thermal Energy of the Lattice Ions}}, \quad (2.16)$$

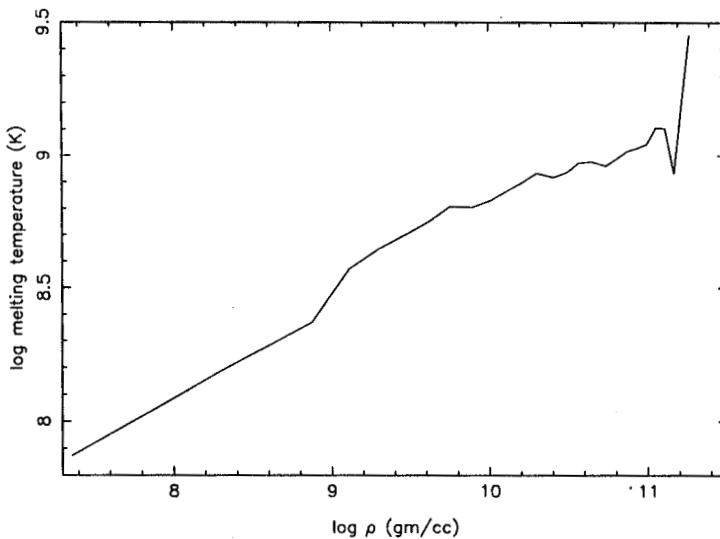


Figure 2.19: Variation of melting temperature with density in the crust on a neutron star.

equals 172 at the melting point. For a crystal composed of ionic species of charge  $Z$  and lattice spacing  $a$ , the Coulomb Energy per ion is  $\frac{(Ze)^2}{a}$  and the thermal energy of an ion is approximately  $k_B T$  where  $T$  is the temperature of the crystal. Therefore,

$$\Gamma = \frac{(Ze)^2}{ak_B T}. \quad (2.17)$$

The inter atomic spacing  $a$ , in terms of density is,

$$a = \left(\frac{4\pi}{3}\right)^{-1/3} \left(\frac{\rho}{A}\right)^{-1/3} m_p^{1/3}, \quad (2.18)$$

$m$  and  $A$  being the proton mass and the mass number of the ion, respectively. Then the melting temperature is

$$T_m = 0.22692 \times 10^8 \frac{Z^2 \left(\frac{\rho_6}{A}\right)^{1/3}}{171} K, \quad (2.19)$$

where  $\rho_6$  is the density in  $10^6 \text{ gm/cc}$ . In figure [2.19] the melting temperature has been plotted versus density in the crust of a  $1.4 M_\odot$  neutron star.

Densities for which the actual temperature is above the melting temperature, the material is in a liquid state. The transport properties in such a state is determined by the electron-ion collisions and by electron-phonon collisions in the solid phase. The three factors important factors in calculating electron-phonon collision time-scale are - the

dielectric screening of the phonon spectrum by the relativistic, Fermi-degenerate electrons, the Debye-Waller factor for the pure Coulomb, bcc crystal and the atomic form factor. The Debye-Waller factor changes the conductivity by a factor of two to four at the melting temperature. And when the electron de-Broglie wavelength becomes comparable to the nuclear size the third correction becomes rather important. Unlike the terrestrial situation, in the crust of a neutron star the Umklapp process dominates. For lower temperatures, the dominant process is that of the collision of electrons with the impurity atoms. These collisions are similar to the electron-ion collision in the liquid phase, except that here the effective charge is the difference between the charge of the impurity atom and the charge of the dominant species. The temperature or density of the cross-over from phonon dominated to impurity dominated process depends on the impurity strength  $Q$ , given by,

$$Q = \frac{1}{n} \sum_i n_i (Z - Z_i)^2, \quad (2.20)$$

where  $n$  is the total ion density,  $n_i$  is the density of impurity species  $i$  with charge  $Z_i$ , and  $Z$  is the ionic charge in the pure lattice (Yakovlev & Urpin 1980).

For our work, we have taken the expression for electrical conductivity of the liquid and due to impurity concentration in the solid from Yakovlev & Urpin (1980). For the pure crystalline phase we have used the results of Itoh et al. (1984). The conductivity in the liquid is given by,

$$\sigma_{\text{liquid}} = 8.53 \times 10^{21} \frac{x^3}{Z \Lambda_{\text{Coulomb}} (1 + x^2)}, \quad (2.21)$$

where  $x$  is defined by the relation

$$x = (Z/\rho_6)^{1/3}, \quad (2.22)$$

and  $\Lambda_{\text{Coulomb}}$  is the Coulomb logarithm. In the solid, the conductivity has contributions from both the phonon and the impurity processes. Therefore, the conductivity is given by,

$$\sigma_{\text{solid}} = \frac{1}{\sigma_{\text{phonon}}^{-1} + \sigma_{\text{impurity}}^{-1}}, \quad (2.23)$$

where

$$\sigma_{\text{impurity}} = 8.53 \times 10^{21} x Z / Q / s \quad (2.24)$$

$$\sigma_{\text{phonon}} = 1.24 \times 10^{20} \frac{x^4 (u^2 + 0.0174)^{1/2}}{u T_8 (1 + 1.018 x^2) I_\sigma}, \quad (2.25)$$

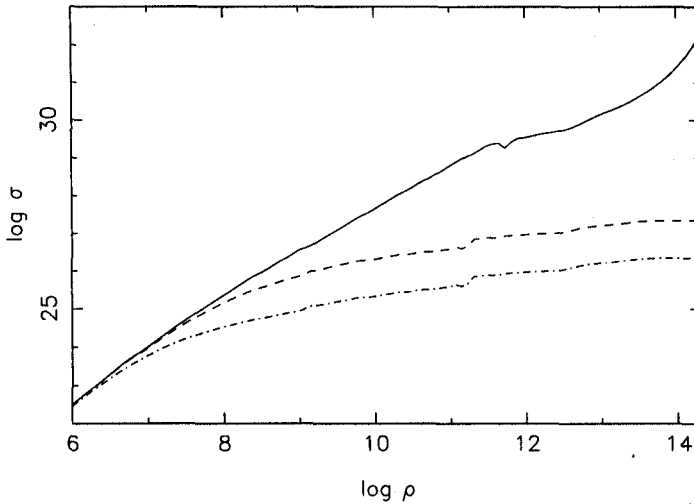


Figure 2.20: Variation of the electrical conductivity with density in the crust of a cool neutron star. The solid, dashed and dash-dotted curves correspond to  $Q = 0.0, 0.01, 0.1$ . For all curves the surface temperature has been taken to be equal to  $10^{4.5}$  K.

with,

$$u = \frac{2\pi}{9}(\log\rho - 3)$$

$$T_8 = \text{temperature in units of } 10^8 \text{ K}$$

$$\rho_6 = \text{density in units of } 10^6 \text{ g cm}^{-3}$$

$$\mathbf{I} = \text{a function of density, } Z, A \text{ given by Itoh et al. 1984.}$$

In the following diagrams we have plotted the electrical conductivity in the crust of a neutron star, as a function of density and emphasizing the dependence on various parameters. In figure [2.20], the plot is for different values of the impurity concentration  $Q$  for a given surface temperature. Notice that in this case we assume a temperature variation with density as is expected in a cool, isolated neutron star (section 2.3). In figure [2.21], on the other hand, we have plotted the conductivity for different values of the temperature which is constant over the whole of the crust. In figure [2.22], we have shown the change in conductivity with different values of  $Q$ , assuming the same constant crustal temperature in each case.

In figures [2.21] and [2.22] we have plotted the conductivity assuming the temperature to be constant over the entire crust. That is the case for a star with an accretion heated

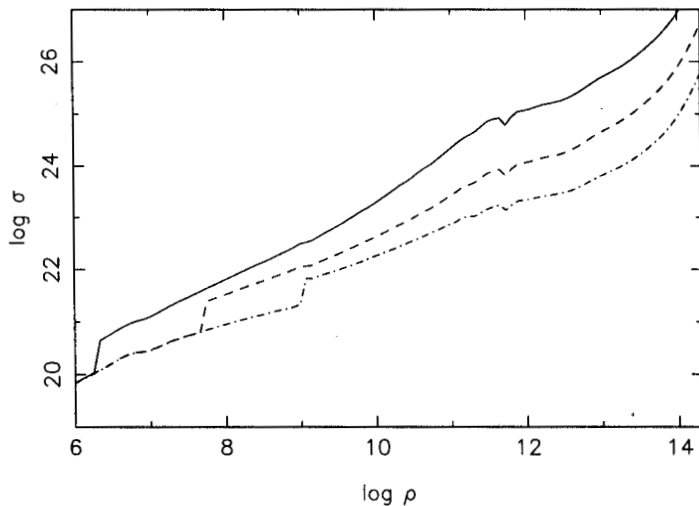


Figure 2.21: Variation of the electrical conductivity with density in the crust of a neutron star. The solid, dashed and dash-dotted curves correspond to the crustal temperatures of  $10^{7.5}$ ,  $10^8$ ,  $10^{8.5}$  K. In all the curves  $Q = 0$ .

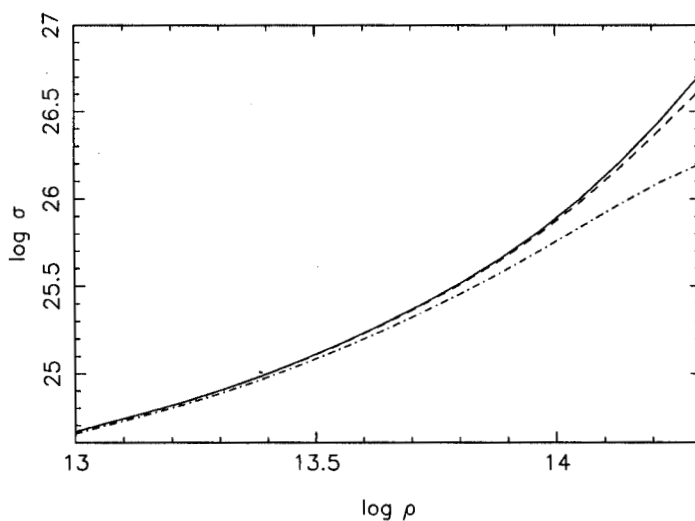


Figure 2.22: Variation of the electrical conductivity with density in the crust of a neutron star. The solid, dashed and dash-dotted curves correspond to  $Q = 0.0, 0.01, 0.1$ . For all curves  $T = 10^8$  K.

crust after the temperature has stabilized. For an isolated star with a very low surface temperature and a non-zero temperature gradient in the outermost layers (as described in section [2.3] above) the variation of conductivity with density looks somewhat different. In figure [2.20] we plot the conductivity profile for such a cool star. Note that the impurity strength  $Q$  becomes important in this case.

It should be mentioned here that the above discussion does not refer to the fact that the transport properties in the crust of a neutron star must also take into account the presence of magnetic fields. As early as in 1980, Urpin & Yakovlev had looked into this problem. And recently, very refined results have been available in which conductivity calculations have been made with magnetic field (Potekhin 1997, Potekhin & Yakovlev 1997). Also, all the above calculations have been made assuming a bcc lattice. Recently, Baiko & Yakovlev (1995) have also investigated the case of fcc lattice. But for our calculations we have not made use of these refined results.